Sound Absorption Optimization of Graded Semi-Open Cellular Metals by Adopting the Genetic Algorithm Method

H. Meng
State Key Laboratory for Strength and Vibration of Mechanical Structures, School of Aerospace, Xi'an Jiaotong University, Xi'an 710049, China

F. X. Xin[1]
State Key Laboratory for Strength and Vibration of Mechanical Structures, School of Aerospace, Xi'an Jiaotong University, Xi'an 710049, China
e-mail: fengxian.xin@gmail.com

T. J. Lu
State Key Laboratory for Strength and Vibration of Mechanical Structures, School of Aerospace, Xi'an Jiaotong University, Xi'an 710049, China

Built upon the acoustic impedance of circular apertures and cylindrical cavities as well as the principle of electroacoustic analogy, an impedance model is developed to investigate theoretically the sound absorption properties of graded (multilayered) cellular metals having semi-open cells. For validation, the model predictions are compared with existing experimental results, with good agreement achieved. The results show that the distribution of graded geometrical parameters in the semi-open cellular metal, including porosity, pore size, and degree of pore opening (DPO), affects significantly its sound absorbing performance. A strategy by virtue of the genetic algorithm (GA) method is subsequently developed to optimize the sound absorption coefficient of the graded semi-open cellular metal. The objective functions and geometric constraint conditions are given in terms of the key geometrical parameters as design variables. Optimal design is conducted to seek for optimal distribution of the geometrical parameters in graded semi-open cellular metals. [DOI: 10.1115/1.4028377]

Keywords: sound absorption, graded semi-open cellular material, optimization, genetic algorithm (GA) method

1 Introduction

Highly porous cellular metals having either full- or semi-open cells have been exploited as sound absorbing materials for a range of noise and vibration control applications, particularly in hostile surroundings [1–9]. Compared with traditional sound absorbent materials such glass wool and polymer foams, aluminum foams are mechanically stiff, strong and stable, do not generate toxic gases in the presence of a flame, have high durability and resistance to weathering, and can shield against electromagnetic waves.

Sound absorption in porous materials has been a subject of significance in many practical applications, and has been studied extensively in the past. When a sound wave propagates across these porous materials, the capability of the material to absorb sound is derived from energy dissipation caused mainly by viscous drag of air and thermal-elastic damping. A relatively small portion of the energy may also be lost via other energy dissipating mechanisms, such as Helmholtz-type resonance, vortex shedding from sharp edges, and direct mechanical damping in the material itself. The analytical model proposed by Biot [10,11] has been widely used to predict the wave propagation behavior across different fluid-saturated porous media [12–14]. Despite the success of Biot's classical model, a variety of alternative theoretical models have been developed to predict the acoustic properties of porous materials. For instance, an empirical model based on experimental measurements was presented by Delany and Bazley [15], in which the characteristic impedance and propagation coefficient of a porous absorbent material were normalized as a function of frequency divided by its static flow-resistance. Relative to the Biot model, the Delany–Bazley model attracted much attention due to its simplicity. As an extension of Delany and Bazley's model, Miki [16] modified the impedance function and the propagation constant so as to achieve better predictions especially for multilayer porous materials. It has nonetheless been well established that, at low frequencies, the use of Delany and Bazley's model could not give accurate or physically realistic predictions. Allard and Champoux [17] subsequently presented a new empirical model for sound propagation in porous absorbent materials and showed that the new model could provide better predictions both at low and high frequencies. With the consideration of surface shape and the perforated plates used as protection, Chen et al. [18] developed an efficient finite element procedure to investigate the sound absorption performance of different porous materials. Further, from the viewpoint of engineering perspective, Brennan and To [19] derived simple nondimensional expressions of the characteristic impedance and wavenumber for sound propagation in rigid-frame porous materials by using the concepts of acoustic mass, stiffness, and damping.

Semi-open cellular metals as a sound absorbent material have attracted increasing attention, due partly to pore morphology designability and convenient manufacturing procedures (e.g., infiltration processing) [5,20]. A typical cellular morphology of the material is presented in Fig. 1. As a key geometric parameter of the material, the DPO is closely related to the infiltration process [20]. By applying the principle of electroacoustic analogy, Lu et al. [5] proposed a theoretical model based on idealized pore morphologies to evaluate the sound absorption performance of this material, and compared model predictions with experimental measurements. Further sound absorption measurements [3] have been conducted to examine the effects of pore size, pore opening, and pore opening density. The underwater sound absorption behavior of the material was also experimentally investigated by Chen et al. [21] using the pulse tube method. The theoretical and experimental results demonstrated that the sound absorption properties of semi-open cellular metals are strongly affected by geometrical parameters such as porosity, pore size, and DPO. This suggests the feasibility of further improving the sound absorption performance of the material by tuning the distributions of key geometrical parameters.

Built upon a microstructural acoustic model, Dupère et al. [22] concluded that the sound absorption capability of cellular materials over a wide range of frequency would be substantially improved with graded porosity and pore size. Experimentally,

[1]Corresponding author.

Contributed by the Noise Control and Acoustics Division of ASME for publication in the Journal of Vibration and Acoustics. Manuscript received June 26, 2013; final manuscript received August 18, 2014; published online September 11, 2014. Assoc. Editor: Lonny Thompson.

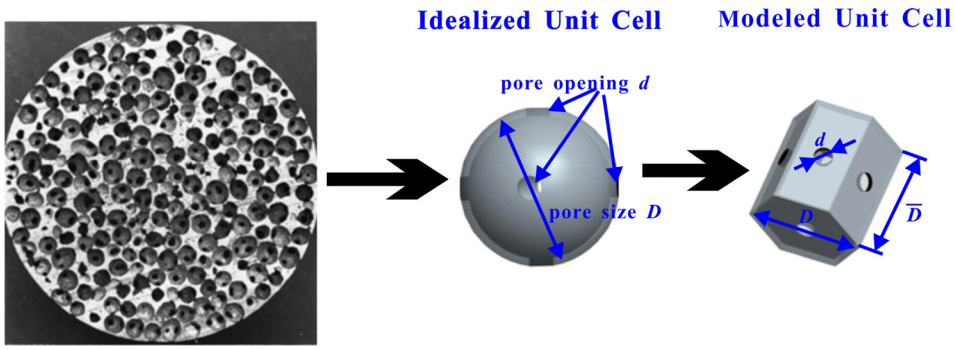

Fig. 1 Idealized unit cell and arrangement for cellular metals having semi-open cells

Huang et al. [7] investigated the effect of pore size distribution in semi-open cellular metals on sound absorption and found that graded pore size led to enhanced sound absorption properties. Despite these efforts, hitherto there is yet a systematic study focusing on the effects of graded distributions of key geometrical parameters (e.g., porosity, pore size, and DPO) upon the sound absorbing capability of semi-open cellular metals. Also, an efficient optimization strategy is needed to provide optimal acoustic design in terms of actual engineering requirements. These deficiencies are squarely addressed in the present study. Based upon idealized cellular morphology consisting of circular apertures and cylindrical cavities as well as the principle of electroacoustic analogy, an impedance acoustic model is first proposed for graded (multilayered) semi-open metallic foams. The model is subsequently employed together with an optimization strategy by virtue of the GA method to provide optimal solutions for semi-open cellular metals as a sound absorbing material.

2 Theoretical Model of Cellular Metal With Semi-Open Cells

Based on the acoustic impedance recursion formula, a theoretical model is established in this section to characterize the sound absorption performance of semi-open cellular aluminum foams (8.0–10.0 wt.% Si, 1.3–1.8 wt.% Cu, 0.4–0.6 wt.% Mg, 0.10–0.35 wt.% Mn, and 0.10–0.35 wt.% Ti) fabricated using the technique of negative-pressure infiltration [5]. To this end, following Lu et al. [5], the semi-open cellular metal may be idealized as one having regularly spaced uniform spherical pores, with uniform circular pore openings at the joints between the pores. For sound vertically incident into the cellular metal, the cellular metal may be further approximated as a regular hexagonal lattice with circular pore opening on each of its eight surfaces as shown in Fig. 1. The model porous material is characterized by pore size D, pore opening d, and porosity Ω. Note that the cell has a coordination number of 8, which is close to the experimentally measured value of 7.0–7.5. Also, although hexagonal arrangement of the pore openings is assumed, the effect of other arrangements such as regular square array or random distribution upon the sound absorption performance of the model material is expected to be small [5].

The diameter of the circumcircle of the hexagonal lattice is equal to the diameter of the spherical pore D, while the height of the hexagonal lattice $\overline{D}$ is set to ensure that the volume of the hexagonal lattice is equal to that of the spherical pore, so that

$$\overline{D} = 0.806D \tag{1}$$

With reference to Fig. 1, $\bar{D}$ is the distance between the middle planes of end walls of the unit cell in the longitudinal direction. For simplicity, the diameter of the circular openings on the surfaces of the unit cell is assumed equal to that of the pore opening of a real porous metal, and that the porosity of the model material is identical to that of the real material. Consequently, the pore connectivity of the model material is identical to that of the real material, namely, $I = d/D$. Besides, uniform cell-wall thickness is assumed and each cell wall is assumed to have identical thickness t. Further, the cell walls are assumed to be sufficiently thin so that $t \ll D$. In terms of pore diameter D and porosity Ω, the cell-wall thickness may be expressed as [5]: $t \approx (1-\Omega)D/(3.55 - 6(d/D)^2)$. Finally, since the density and stiffness of the metal skeleton are much larger than those of air, the skeleton is regarded as motionless as sound propagates across the cellular metal [23].

Consider first a model cellular foam with only one cell in the thickness direction (also the direction of sound propagation). With the wavelength of the sound traveling in air assumed much larger than D and that the sound wave is normally impinging upon the foam surface, the impedance z_0 of the circular pore opening may be calculated by applying the principle of electroacoustic analogy and the relevant formula for the acoustic impedance of a small, circular orifice in a thin plate, as [5,24]

$$z_0 = R_0 + iM_0 \tag{2}$$

where R_0 and M_0 are functions of the acoustic Reynolds number $\beta = \sqrt{\omega\rho_0/\eta}d/2$, the latter determined by the quotient of two stresses induced separately by sound pressure and viscosity. Here, ρ_0 is the density of air, ω is the frequency of the incident sound, η is the dynamic viscosity of air, and d is the diameter of the pore opening (Fig. 1). For $\beta < 1$ (low-frequency range or small circular opening)

$$R_0 = 32\eta t/d^2 \tag{3}$$

$$M_0 = (4/3)\omega\rho_0 t \tag{4}$$

When $1 < \beta < 10$ (intermediate frequency range)

$$R_0 = \frac{32\eta t}{d^2}\sqrt{1+\beta^2/32} \tag{5}$$

$$M_0 = \omega\rho_0 t\left\{1 + 1/\sqrt{9+\beta^2/2}\right\} \tag{6}$$

When $\beta > 10$ (high-frequency range or large circular opening)

$$R_0 = 8\eta t\beta/\sqrt{2}d^2 \tag{7}$$

$$M_0 = \left(8\eta t\beta/\sqrt{2}d^2 + \omega\rho_0 t\right) \tag{8}$$

Since the end effect of the pore openings should be considered for short tubes [24,25], the cell-wall thickness t needs to be corrected by an end correction $a = 8d/3\pi$ when $\beta < 1$ or $\beta > 10$. Thus, t is replaced by the effective thickness t', as [25]

$$t' = t + a \tag{9}$$

Accordingly, Eqs. (3) and (4) become

$$R_0 = 32\eta\left(t+\frac{8d}{3\pi}\right)/d^2 \tag{10}$$

$$M_0 = (4/3)\omega\rho_0\left(t+\frac{8d}{3\pi}\right) \tag{11}$$

while Eqs. (12) and (13) become

$$R_0 = 8\eta\left(t+\frac{8d}{3\pi}\right)\beta/\sqrt{2}d^2 \tag{12}$$

$$M_0 = 8\eta\left(t+\frac{8d}{3\pi}\right)\beta/\sqrt{2}d^2 + \omega\rho_0\left(t+\frac{8d}{3\pi}\right) \tag{13}$$

Similarly, with the end effect added to Eqs. (5) and (6) for $1 < \beta < 10$, the acoustic impedance of the pore opening becomes [24]

$$R_0 = \frac{32\eta t}{d^2}\left\{\sqrt{1+\beta^2/32}+\sqrt{\beta d/4t}\right\} \tag{14}$$

$$M_0 = \omega\rho_0 t\left\{1+1/\sqrt{9+\beta^2/2}+0.85d/t\right\} \tag{15}$$

In addition to the acoustic impedance of pore openings, the impedance of air inside the hexagonal cells Z_D needs to be determined. To this end, the hexagonal prismatic pore of Fig. 1 is modeled by a circular cylindrical pore of equal cross-sectional area, so that its diameter $\overline{D_c} = 0.909D$. Under such conditions

$$Z_D = -i\rho_0 c_0 \cot\left(\omega\overline{D_c}/c_0\right) \tag{16}$$

where c_0 is the sound speed in air.

Consider next a semi-open foam sample consisted of k layers of unit cells, as shown in Fig. 2, with total thickness L. As graded foams are of concern, the unit cell may vary from one layer to another. With the sample backed by a rigid wall, its acoustic impedance may be calculated by employing the recursion formula, as [5]

$$Z^{(k)} = \begin{cases} Z_0^{(k)} + \dfrac{1}{\dfrac{1}{Z_D^{(k)}}+\dfrac{1}{Z^{(k-1)}}}, & k \geq 2 \\ Z_0^{(1)} + Z_D^{(1)}, & k = 1 \end{cases} \tag{17}$$

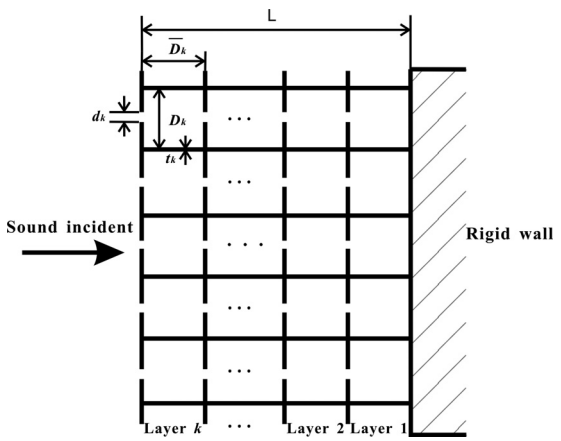

Fig. 2 Schematic of a semi-open cellular metal sample with k layers backed by rigid wall

where $Z_0^{(k)} = z_0^{(k)}\left(\bar{D}_c^{(k)}/d^{(k)}\right)^2$ is the relative specific acoustic impedance of air in the pore openings of the kth layer with $D_c^{(k)}$ and $d^{(k)}$ representing the equivalent cylindrical pore diameter and the pore opening diameter of the kth layer, respectively, $z_0^{(k)}$ is the impedance of circular pore openings of the kth layer, $Z_D^{(k)}$ is the impedance of air in the cells of the kth layer, and $Z^{(k-1)}$ is the impedance of the sample made of $k-1$ layers.

Finally, the sound absorption coefficient α of the semi-open foam sample made of k layers (Fig. 2) is obtained as

$$\alpha = \frac{4R/\rho_0 c_0}{\left(1+R/\rho_0 c_0\right)^2 + \left(M/\rho_0 c_0\right)^2} \tag{18}$$

where $R = \mathrm{Re}\left(Z^{(k)}\right)$ and $M = \mathrm{Im}\left(Z^{(k)}\right)$ are the resistance and reactance of the impedance for the whole k layers, respectively.

To validate the theoretical model as formulated above, Fig. 3 compares the predicted sound absorption coefficient for a 6-layer graded semi-open foam sample with the experimental results of Huang et al. [7]. The sample was backed by a rigid wall (i.e., no air gap between the sample and the back plate). The geometrical parameters used are identical to those provided in Ref. [7]: the pore size of the 6-layer graded cellular metal varies as (0.8, 1.0, 1.2, 1.4, 1.8, and 2.2) mm; each layer containing uniform pores has a fixed thickness of 3 mm and a fixed porosity of 66%. The results shown in Fig. 3 demonstrate that overall the model predictions agree well with experimental measurements, capturing accurately the peak at 2000 Hz and the dip at 4000 Hz. The small discrepancy between theory and experiment may be attributed to the idealized nature of the theoretical model used to describe the actual graded semi-open cellular metal.

3 Optimization of Graded Cellular Metals With Semi-Open Cells

Built upon the theoretical model detailed in Sec. 2, we present here a sound absorption optimization procedure for graded cellular metals having semi-open cells. The effects of relevant geometric parameters upon sound absorption are first examined to determine the key optimal design variables. Suitable objective functions and constraints are subsequently developed, whilst the method of GA as outlined in the Appendix is adopted to solve the corresponding optimization problems.

It can be drawn from the present theoretical model that the sound absorption property of a semi-open cellular metal is mainly determined by three geometric parameters, i.e., circular pore

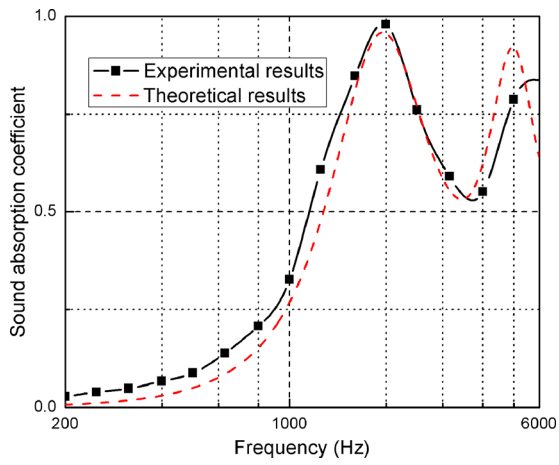

Fig. 3 Sound absorption of 6-layer graded semi-open cellular metal: comparison between model predictions and experimental measurements [7]

opening diameter d, spherical cell diameter D, and porosity Ω, which provide a broad space for sound absorption optimization of the cellular metal. However, since the DPO $\delta = d/D$ is frequently used during material processing [20], d is replaced here by the dimensionless δ.

Before proceeding further, with the volume (height) and weight of semi-open cellular metal samples fixed, the distribution of one of the three design variables (porosity, pore size, and DPO) in the sample is varied while the two others remain unchanged (Table 1) so as to explore towards which direction optimal sound absorption may be achieved. The results are shown in Figs. 4–6 in terms of sound absorption coefficient versus frequency curves. All the samples are backed by a rigid wall, as illustrated schematically in Fig. 2.

Table 1 Geometrical parameters of semi-open cellular metal samples

Samples	Porosity Ω (%)	Pore size D (mm)	DPO δ	Thickness H (mm)
a	60	1.24	0.3	10
b	50|70	1.24	0.3	10
c	40|60|80	1.24	0.3	10
d	60	1.04|1.44	0.3	10
e	60	0.84|1.24|1.64	0.3	10
f	60	1.24	0.25|0.35	10
g	60	1.24	0.2|0.3|0.4	10

Note: "|" denotes the boundary between two different layers.

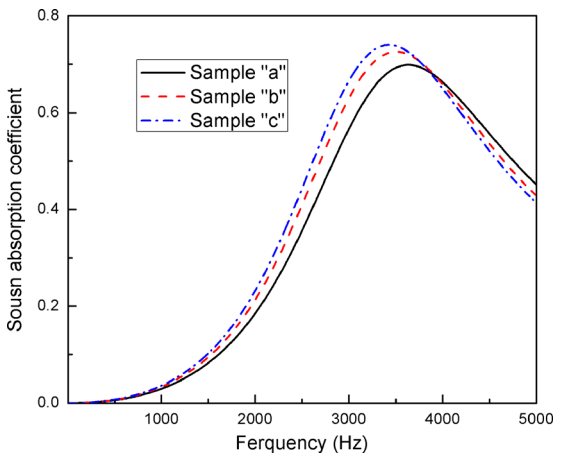

Fig. 4 Comparison of sound absorption coefficient between semi-open cellular foam samples having different porosity distributions

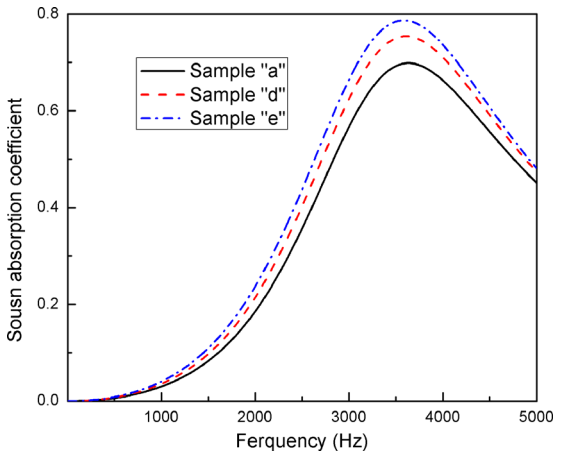

Fig. 5 Comparison of sound absorption coefficient between semi-open cellular foam samples having different pore size distributions

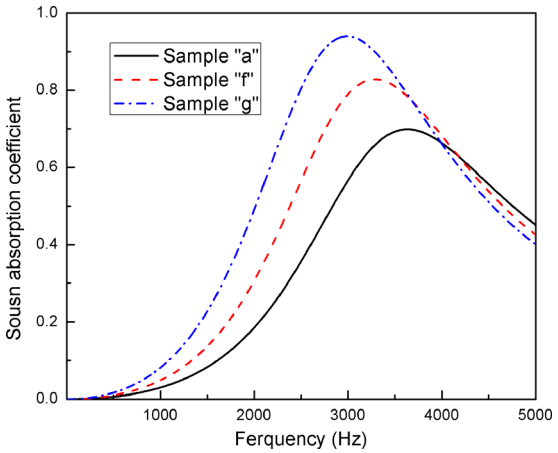

Fig. 6 Comparison of sound absorption coefficient between semi-open cellular foam samples having different DPO distributions

As can be seen from Fig. 4, how porosity is distributed in the semi-open cellular metal affects significantly its sound absorption performance. Within the frequency range of interest, the sound absorption coefficient is noticeably increased as the porosity gradation level (e.g., toward continuously graded distribution in the case of infinite number of layers) is increased. Similarly, the results of Figs. 5 and 6 demonstrate that the distribution of pore size or DPO also plays an important role, with sound absorption increasing as the gradation level of each parameter is increased, particularly so in the case of DPO. It appears therefore that there exists a large design window to tune the distribution(s) of porosity, pore size, and DPO so that the sound absorption performance of a semi-open cellular metal may be optimized, as discussed in detail next. It is worth noting here that whilst sole frequency optimization is preferable for simplicity, it is also meaningful to perform optimization over a certain frequency range. Both possibilities will be explored.

3.1 Optimization of Porosity Distribution. To optimize the distribution of porosity in multilayered semi-open cellular metals at a sole frequency, the objective function for sound absorption coefficient α may be written as

$$\min\ f(\mathbf{\Omega}) = 1 - \alpha(\mathbf{\Omega}) \tag{19}$$

where $\mathbf{\Omega} = [\Omega_1, \Omega_2, \Omega_3, ..., \Omega_n]$ represents the porosity of each layer and n is the total number of layers.

Given an expected porosity of a graded sample, the restriction of same mass and volume as the uniform (ungraded) sample requires that the average of the optimized porosity is equal to the expected porosity. Besides, the porosity should be bigger than zero but smaller than one. Therefore, the constraints of the objective function may be written as

$$\begin{aligned} &\text{s.t. } 0 < \Omega_1, \Omega_2, ..., \Omega_n < 1 \\ &\sum_{i=1}^{n} \Omega_i / n \approx \Omega \end{aligned} \tag{20}$$

where Ω is the expected averaged porosity since both the mass and volume of the sample are fixed.

As to porosity optimization within a prespecified frequency range, the objective function may be developed by minimizing the

margin of calculated sound absorption coefficients within the frequency range, as

$$\min\ f(\alpha_1(\mathbf{\Omega}), \alpha_2(\mathbf{\Omega}), \alpha_3(\mathbf{\Omega}), ..., \alpha_m(\mathbf{\Omega})) = \sqrt{\sum_{i=1}^{m} (\alpha_i(\mathbf{\Omega}) - 1)^2} \tag{21}$$

The constraints are the same as the case of sole frequency optimization, Eq. (24).

3.2 Optimization of Pore Size Distribution. The optimization of pore size distribution is conducted exactly as the optimization of porosity distribution. The objective function for sole frequency optimization is

$$\min\ f(\mathbf{D}) = 1 - \alpha(\mathbf{D}) \tag{22}$$

where $\mathbf{D} = [D_1, D_2, D_3, ..., D_n]$ represents the pore size of each layer.

In order to compare with a uniform sample with identical mass and volume, there should exist a geometric constraint between the sum of the optimized pore size and the expected sample thickness. Moreover, while the lower bound of the pore size is 0 mm in theory, the manufacturing process of the material dictates that the pore size cannot be too small because of the surface tension of the molten metal. Practically, for semi-open aluminum foams considered in the present study, the minimum pore size was approximately 0.8 mm [7]. Thus, the constraints of the objective function for pore size optimization are

$$\begin{aligned} &\text{s.t. } 0.806 \sum_{i=1}^{n} D_1 \approx H \\ &D_1, D_2, ..., D_n > 0.8 \end{aligned} \tag{23}$$

where H is the expected sample thickness.

For optimization within a certain frequency range, the objective function is

$$\min\ f(\alpha_1(\mathbf{D}), \alpha_2(\mathbf{D}), \alpha_3(\mathbf{D}), ..., \alpha_m(\mathbf{D})) = \sqrt{\sum_{i=1}^{m} (\alpha_i(\mathbf{D}) - 1)^2} \tag{24}$$

which is subjected to the same constraints of Eq. (23).

3.3 Optimization of DPO Distribution. The objective function for DPO optimization at a sole frequency may be written as

$$\min\ f(\boldsymbol{\delta}) = 1 - \alpha(\boldsymbol{\delta}) \tag{25}$$

where $\boldsymbol{\delta} = [\delta_1, \delta_2, ..., \delta_n]$ represents the DPO of each layer.

Since the circular pore opening has a diameter d smaller than that of the spherical pore D, the DPO should be bigger than zero but smaller than one. Further, the wall thickness of the unit cell should be bigger than zero but smaller than the radius of the pore. Therefore, the constraints are

$$\begin{aligned} &\text{s.t. } 0 < \delta_1, \delta_2, ..., \delta_n < 1 \\ &0 < t_i \approx \frac{(1-\Omega)D}{3.55 - 6\delta_i^2} < \frac{D}{2}, \quad i = 1, 2, ..., n \end{aligned} \tag{26}$$

For DPO optimization within a certain frequency range, the objective function is

$$\min\ f(\alpha_1(\boldsymbol{\delta}), \alpha_2(\boldsymbol{\delta}), \alpha_3(\boldsymbol{\delta}), ..., \alpha_m(\boldsymbol{\delta})) = \sqrt{\sum_{i=1}^{m} (\alpha_i(\boldsymbol{\delta}) - 1)^2} \tag{27}$$

subjected to the same constraints of Eq. (26).

Since the six objective functions given above are all complex multimodal nondifferentiable functions, the commonly used gradient method cannot be employed. As a powerful alternative, the GA method (see Appendix) is applied instead.

4 Numerical Results and Discussions

On the basis of the proposed acoustic model for multilayer semi-open cellular metals and the optimization strategy, numerical calculations are carried out below to evaluate the feasibility of the theoretical model as well as the GA optimization strategy.

4.1 Optimized Porosity Distribution. This part aims to identify the porosity distribution in a foam sample that may maximize its sound absorption subjected to the constraints of identical mass and volume. Here, the semi-open foam sample to be optimized is 10 mm thick, with fixed pore size of 1.24 mm and fixed DPO of 0.2 for each layer, while the expected averaged porosity is 70%. The number of the layers is

$$n \approx \frac{L}{0.806D} = \frac{10}{0.806 \times 1.24} = 10 \tag{28}$$

The optimization of porosity distribution is conducted following the process of the GA strategy outlined in the Appendix. The final optimization results are presented in Table 2, both for the sole frequency of 2000 Hz and the frequency range of 2000–2500 Hz. For comparison, results corresponding to uniform as well as linear porosity distributions are also given in Table 2. Built upon the porosity distributions listed in Table 2, Fig. 7 compares the sound absorption coefficient as a function of frequency for samples having uniform porosity distribution, linear porosity distribution, and sole-frequency optimized porosity distribution, respectively. The corresponding results for porosity distribution optimized within the frequency range of 2000–2500 Hz are

Table 2 Typical porosity distributions for semi-open cellular metal samples

Layer	1	2	3	4	5	6	7	8	9	10
Uniform (%)	70	70	70	70	70	70	70	70	70	70
Linear (%)	61	63	65	67	69	71	73	75	77	79
Optimized at 2000 Hz (%)	70	89	89	89	89	89	90	18	61	18
Optimized at 2000–2500 Hz (%)	66	89	98	90	84	71	87	57	29	27

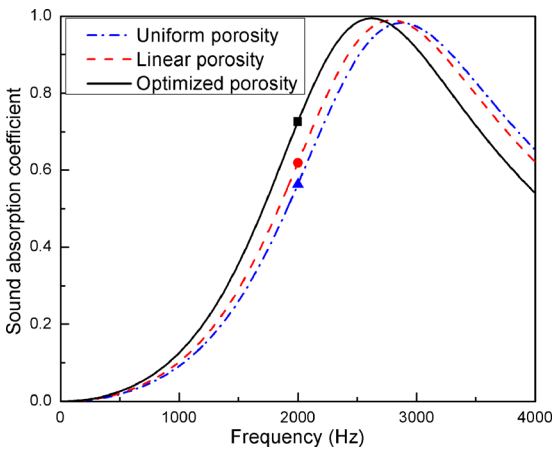

Fig. 7 Predicted sound absorption coefficient plotted as a function of frequency for semi-open cellular metal: comparison amongst uniform, linear, and sole-frequency (2000 Hz) optimized porosity distributions

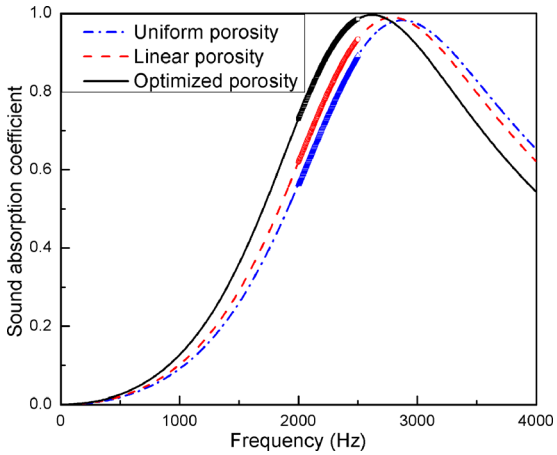

Fig. 8 Predicted sound absorption coefficient plotted as a function of frequency for semi-open cellular metal: comparison amongst uniform, linear, and frequency-range (2000–2500 Hz) optimized porosity distributions

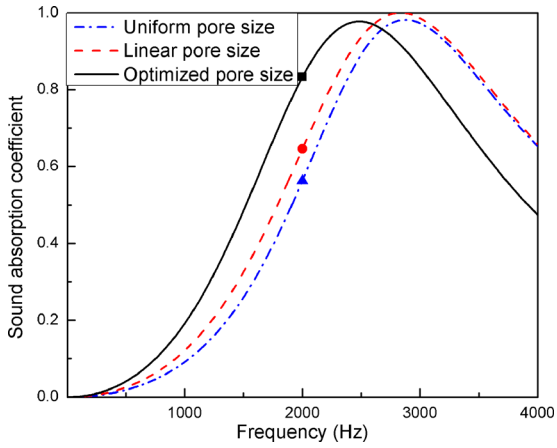

Fig. 9 Sound absorption coefficient of semi-open cellular metal material: comparison amongst uniform, linear, and sole-frequency (2000 Hz) optimized pore size distributions

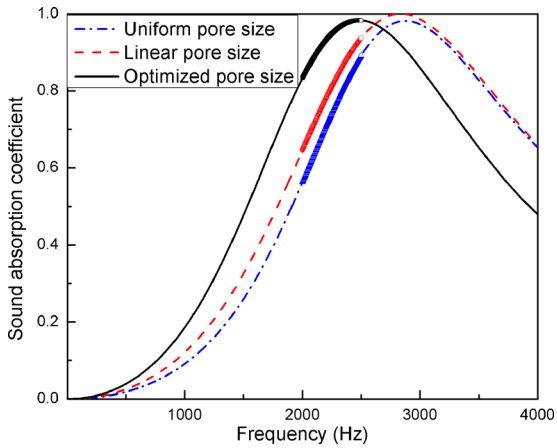

Fig. 10 Sound absorption coefficient of semi-open cellular metal material: comparison amongst uniform, linear, and frequency-range (2000–2500 Hz) optimized pore size distributions

compared with nonoptimized results in Fig. 8. Here, the simplest graded porosity distribution (i.e., linear porosity distribution) is selected to highlight the superiority of the present optimization strategy based on the GA method.

It can be seen from Fig. 7 that, relative to samples having either uniform or linear porosity distribution, the sample having sole-frequency optimized porosity distribution exhibits not only higher sound absorption at the sole frequency of 2000 Hz but also within a wide frequency range of interest (approximately below 2700 Hz). The same conclusion holds for samples having frequency-range optimized porosity distributions, as shown in Fig. 8.

4.2 Optimized Pore Size Distribution. Consider next the optimal design of pore size distribution for 10 mm thick semi-open foam samples having fixed porosity of 70%, fixed DPO of 0.2 for each layer and a total of 10 layers. Given the objective function and the constraint conditions of Eqs. (22) and (23), the GA method can effectively search for the optimal pore size distribution. The final results for both sole-frequency (2000 Hz) and frequency-range (2000–2500 Hz) optimization are listed in Table 3, together with the results for samples having uniform and linear pore size distributions. Note that for a uniform sample, the thickness of each layer is 1 mm, so that the pore size of each layer can be calculated by Eq. (1) as

$$D_{\text{aver}} = \frac{1}{0.806} = 1.24\,\text{mm} \tag{29}$$

For a sample with optimized pore size distribution, however, the thickness of each layer becomes unequal since the pore size of each layer is altered to some extent as a result of optimization. Nonetheless, the thickness of each layer may still be estimated using Eq. (1).

With the pore size distributions listed in Table 3, the predicted sound absorption coefficient of semi-open cellular metals are presented in Figs. 9 and 10 for sole-frequency optimization and frequency-range optimization, respectively. The optimized pore size distribution enhances significantly the sound absorption capability not only at the selected frequencies (i.e., 2000 Hz in Fig. 9 and 2000–2500 Hz in Fig. 10) but also over a wide frequency range, especially at low frequencies (below 2500 Hz). Moreover, the noticeable increase of sound absorption coefficient implies that the pore size can be taken a key design parameter for this kind of sound absorbing porous material.

4.3 Optimized DPO Distribution. Consider next the DPO as a design parameter for semi-open foam samples having 10 mm in thickness, with fixed porosity of 70% and fixed pore size of 1.24 mm. Under such circumstances, the number of layers in each sample is estimated as 10. Table 4 lists the sole-frequency (2000 Hz) and frequency-range (2000–2500 Hz) optimization results for

Table 3 Typical pore size distributions for semi-open cellular metal samples

Layer	1	2	3	4	5	6	7	8	9	10
Uniform (mm)	1.24	1.24	1.24	1.24	1.24	1.24	1.24	1.24	1.24	1.24
Linear (mm)	1.69	1.59	1.49	1.39	1.29	1.19	1.09	0.99	0.89	0.79
Optimized at 2000 Hz (mm)	5.2	1.79	0.8	0.8	0.8	0.8	0.8	0.8	0.8	0.8
Optimized at 2000–2500 Hz (mm)	5.2	0.8	0.8	1.78	0.82	0.8	0.8	0.81	0.8	0.8

Table 4 Typical DPO distributions for semi-open cellular metal samples

Layer	1	2	3	4	5	6	7	8	9	10
Uniform	0.24	0.24	0.24	0.24	0.24	0.24	0.24	0.24	0.24	0.24
Linear	0.33	0.31	0.29	0.27	0.25	0.23	0.21	0.19	0.17	0.15
Optimized at 2000 Hz	0.26	0.2	0.63	0.26	0.23	0.2	0.14	0.24	0.11	0.14
Optimized at 2000–2500 Hz	0.24	0.2	0.52	0.37	0.26	0.38	0.20	0.11	0.14	0.17

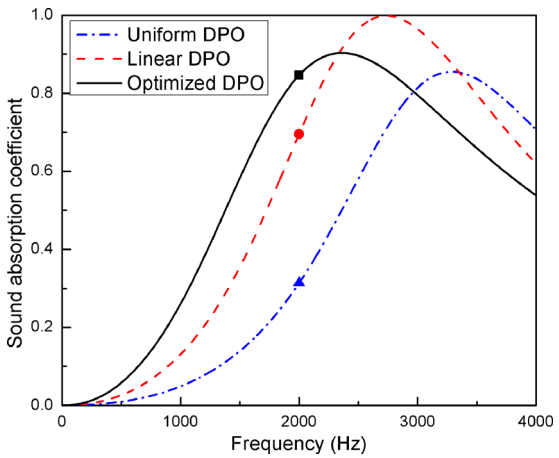

Fig. 11 Sound absorption coefficient of semi-open cellular metal: comparison amongst uniform, linear, and sole-frequency (2000 Hz) optimized DPO distributions

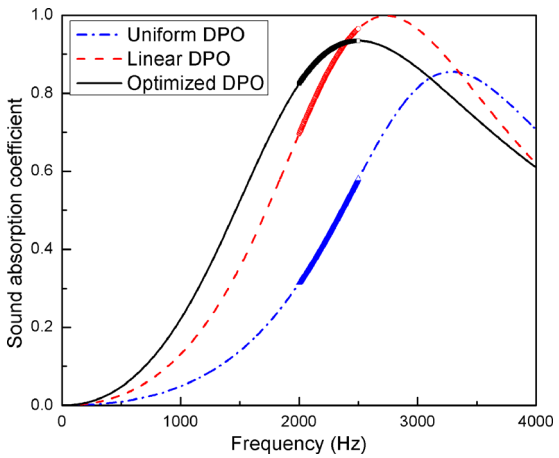

Fig. 12 Sound absorption coefficient of semi-open cellular metal: comparison amongst uniform, linear, and frequency-range (2000–2500 Hz) optimized DPO distributions

DPO distribution. For comparison, the corresponding results for uniform and linear DPO distributions are also presented in Table 4.

Based upon the DPO distributions of Table 4, the predicted sound absorption coefficients of different semi-open foam samples are plotted in Figs. 11 and 12 for sole-frequency optimization and frequency-range optimization, respectively. Relative to uniform and linear DPO distributions, the most significant trend of the curve corresponding to the case of DPO distribution is the dramatic increase of the sound absorption coefficient over the wide frequency range (approximately below 2400 Hz). This again displays the superiority of the developed optimization strategy, which not only achieve enhanced sound absorption at the selected sole frequency but also over the frequency range of interest.

It should be pointed out that, the sound absorption of the linear case within the frequency range of 2400–2500 Hz is higher than that of the optimized case (see Fig. 12), which actually falls into the optimized frequency range of 2000–2500 Hz. However, this does not violate the optimal objective for maximum sound absorption because, within the optimized frequency range of 2000–2500 Hz, the averaged sound absorption of the optimized case still exceeds that of the linear case.

5 Conclusions

Built upon the acoustic impedance of circular apertures and cylindrical cavities as well as the principle of electroacoustic analogy, an impedance model is proposed to describe the sound absorption performance of cellular metallic foams having semi-open cells; the model predictions agree well with existing experimental measurements. To optimize the acoustic property of graded semi-open foams, an optimization strategy on the basis of the GA method is developed to define the objective functions and geometric constraint conditions in terms of key morphological parameters as design variables, including the porosity, the pore size, and the DPO. To highlight the efficiency of the optimization strategy, uniform and linear distributions of the design variables are also considered subjected to the constraint of same mass and volume. It is demonstrated that, in terms of sound absorption, the graded distribution of each design variable is superior to uniform or linear distribution not only in the optimized frequency range but also in a wide frequency range of interest. Whilst the distributions of porosity, pore size, and DPO in semi-open metal foams can all be tuned for optimized sound absorption performance, the effects of pore size and DPO optimization are more significant than that of porosity.

Acknowledgment

This work was supported by the National Basic Research Program of China (Grant No. 2011CB6103005), the National Natural Science Foundation of China (Grant Nos. 11102148 and 11321062), and the Fundamental Research Funds for Central Universities (Grant No. xjj2011005).

Appendix: Summary of the GA Method

The GA method is composed of eight parts, which can be schematically shown as

$$\mathrm{GA} = (C, E, P_0, N, \Phi, \Gamma, \Psi, T) \tag{A1}$$

Here, C is the encoding method of the individual, which mostly adopts the binary coding method as the encoding method to form a string. Then, the GA method can be favorably started with a population of strings. E is the fitness evaluation function, whose value decides the probability of individuals contributing to the next generation. P_0 is the initial population, which is generated randomly at first. The number of the population size N usually ranges from 20 to 100. The reproduce operator Φ is produced by creating a roulette wheel, where each string has an assigned proportion to its fitness value. The proportion decides the probability of each string to be selected as parent generation for the next generation, which can be calculated as

$$P_i = \frac{f_i}{\sum_{i=1}^{m} f_i} \tag{A2}$$

After reproduction, the sixth term Γ represents the crossover operator and proceeds as follows (as schematically illustrated in Fig. 13): first, mated individuals are generated randomly in the mating pool; afterwards a crossing point should be chosen, the

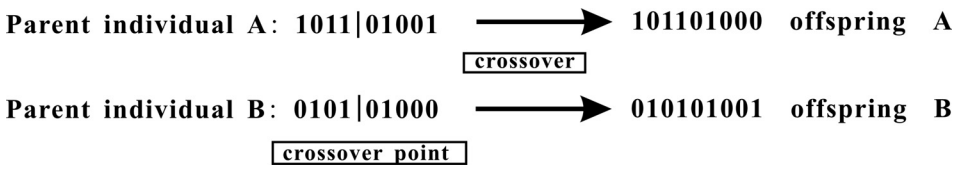

Fig. 13 Schematic diagram of crossover in GA method

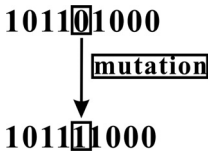

Fig. 14 Schematic diagram of mutation in GA method

codes after which are then exchanged; as a consequence, a new generation can be favorably born. In this process, the probability of the crossover generally ranges from 0.4 to 0.99.

The seventh term Ψ denotes the mutation operator, which defines the occurrence of the mutation to follow the mutation probability in the encoding string randomly, and then the codes are changed at the mutation points. When the binary coding method is applied, the mutation simply produces negate at the mutation point. The probability of the mutation generally ranges from 0.0001 to 0.1. The mutation is depicted in Fig. 14.

The finial term T signifies the terminating conditions. There are many terminating conditions for the GA method in terms of the maximum number of generations, maximum execution time, the fitness value reaching the required threshold and so on.

References

[1] Hakamada, M., Kuromura, T., Chen, Y., Kusuda, H., and Mabuchi, M., 2006, "Sound Absorption Characteristics of Porous Aluminum Fabricated by Spacer Method," J. Appl. Phys., **100**(11), p. 114908.

[2] Lu, T. J., Hess, A., and Ashby, M. F., 1999, "Sound Absorption in Metallic Foams," J. Appl. Phys., **85**(11), pp. 7528–7539.

[3] Li, Y. J., Wang, X. F., Wang, X. F., Ren, Y., Han, F., and Wen, C., 2011, "Sound Absorption Characteristics of Aluminum Foam With Spherical Cells," J. Appl. Phys., **110**(11), p. 113525.

[4] Davies, G., and Zhen, S., 1983, "Metallic Foams: Their Production, Properties, and Applications," J. Mater. Sci., **18**(7), pp. 1899–1911.

[5] Lu, T. J., Chen, F., and He, D. P., 2000, "Sound Absorption of Cellular Metals With Semiopen Cells," J. Acoust. Soc. Am., **108**(4), pp. 1697–1709.

[6] Han, F. S., Seiffert, G., Zhao, Y. Y., and Gibbs, B., 2003, "Acoustic Absorption Behaviour of an Open-Celled Aluminium Foam," J. Phys. D-Appl. Phys., **36**(3), pp. 294–302.

[7] Huang, K., Yang, D. H., He, S. Y., and He, D. P., 2011, "Acoustic Absorption Properties of Open-Cell Al Alloy Foams With Graded Pore Size," J. Phys. D-Appl. Phys., **44**(36), p. 365405.

[8] Gibson, L. J., and Ashby, M. F., 1999, *Cellular Solids: Structure and Properties*, 2nd ed., Cambridge University Press, Cambridge, UK, p. 283.

[9] Lefebvre, L. P., Banhart, J., and Dunand, D., 2008, "Porous Metals and Metallic Foams: Current Status and Recent Developments," Adv. Eng. Mater., **10**(9), pp. 775–787.

[10] Biot, M. A., 1956, "Theory of Propagation of Elastic Waves in a Fluid-Saturated Porous Solid. I. Low-Frequency Range," J. Acoust. Soc. Am., **28**(2), pp. 168–178.

[11] Biot, M. A., 1956, "Theory of Propagation of Elastic Waves in a Fluid-Saturated Porous Solid. II. Higher Frequency Range," J. Acoust. Soc. Am., **28**(2), pp. 179–191.

[12] Geertsma, J., and Smit, D., 1961, "Some Aspects of Elastic Wave Propagation in Fluid-Saturated Porous Solids," Geophysics, **26**(2), pp. 169–181.

[13] Hovem, J. M., and Ingram, G. D., 1979, "Viscous Attenuation of Sound in Saturated Sand," J. Acoust. Soc. Am., **66**(6), pp. 1807–1812.

[14] Hosokawa, A., and Otani, T., 1997, "Ultrasonic Wave Propagation in Bovine Cancellous Bone," J. Acoust. Soc. Am., **101**(1), pp. 558–562.

[15] Delany, M. E., and Bazley, E. N., 1970, "Acoustical Properties of Fibrous Absorbent Materials," Appl. Acoust., **3**(2), pp. 105–116.

[16] Miki, Y., 1990, "Acoustical Properties of Porous Materials—Modifications of Delany–Bazley Models," J. Acoust. Soc. Jpn. E, **11**(1), pp. 19–24.

[17] Allard, J.-F., and Champoux, Y., 1992, "New Empirical Equations for Sound Propagation in Rigid Frame Fibrous Materials," J. Acoust. Soc. Am., **91**(6), pp. 3346–3353.

[18] Chen, W. H., Lee, F. C., and Chiang, D. M., 2000, "On the Acoustic Absorption of Porous Materials With Different Surface Shapes and Perforated Plates," J. Sound Vib., **237**(2), pp. 337–355.

[19] Brennan, M., and To, W., 2001, "Acoustic Properties of Rigid-Frame Porous Materials—An Engineering Perspective," Appl. Acoust., **62**(7), pp. 793–811.

[20] Chen, F., Zhang, A., and He, D. P., 2001, "Control of the Degree of Pore-Opening for Porous Metals," J. Mater. Sci., **36**(3), pp. 669–672.

[21] Cheng, G. P., He, D. P., and Shu, G. J., 2001, "Underwater Sound Absorption Property of Porous Aluminum," Colloids Surf., A, **179**, pp. 191–194.

[22] Dupère, I. D. J., Lu, T. J., and Dowling, A. P., 2007, "Microstructural Optimization of Cellular Acoustic Materials," J. Xi'an Jiaotong Univ., **41**(11), pp. 1251–1256. (in Chinese).

[23] Tang, H. P., Zhu, J. L., Ge, Y., Wang, J. Y., and Lee, C., 2007, "Sound Absorbing Characteristics of Fibrous Porous Materials Gradient Structure," Rare Metal Mater. Eng., **36**(12), pp. 2220–2223. (in Chinese).

[24] Maa, D.-Y., 1987, "Microperforated-Panel Wideband Absorbers," Noise Control Eng. J., **29**(3), pp. 77–84.

[25] Stinson, M. R., and Shaw, E., 1985, "Acoustic Impedance of Small, Circular Orifices in Thin Plates," J. Acoust. Soc. Am., **77**(6), pp. 2039–2042.